CLASSIFICATION OF FEATURES IN HIGH-RESOLUTION AERIAL PHOOTOGRAPHS USING NEURAL NETWORKS

Adam Iwaniak, Tomasz Kubik, Witold Paluszyński, Przemysław Tymków

Institute of Cybernetics Engineering, Wroclaw University of Technology, Janiszewskiego 11/17, Wroclaw, Poland
Agricultural University of Wroclaw, Norwida 25/27, Wroclaw 50-372, Poland
E-mail: iwaniak@ar.wroc.pl, {tkubik|Witold.Paluszynski}@ict.pwr.wroc.pl, przemyslaw.tymkow@wp.pl

ABSTRACT

The aim of this project was to design a technology for automatic regions recognition and classification in raster images, such as high-resolution aerial photographs. For this purpose feed-forward, multi-layer neural networks were employed, trained with manually created reference datasets. The inputs in the training and testing patterns were created from the original images by taking pixels colors (color features or pixels intensities), augmented with local statistics (texture features from GLCM method). The outputs were collected from images classified by hand.
The experiments were done with color aerial photographs, taken with 1m and 0.5m resolution. The results were evaluated by comparing images processed by neural networks with reference manually classified images. The evaluation ranged from good (water and some types of forests) to barely acceptable (urban areas or roads). A strong correlation was observed between the size of field provided to the neural network and the size of the spatial feature.

INTRODUCTION

In the 21st century information collecting and processing is not possible without support of computer systems. Special cases of these are Geographical Information Systems, which are dedicated to work with geospatial data. In Poland the work is in progress on the National Geographical Information System. One of the components in the system's design is the Topographic Data Base (TDB). This component is responsible for doing several tasks, including topographic data collection on the regional level. It contains topographic objects related to the topographic maps in 1:10000 scales. By assumption these objects are retrieved from actual orthophotomaps.
Poland's joining the European Community and its participation in the IACS project came out with a strong help in TDB implementation. Within the scope of the IACS project it is expected that around 20% of the country will have a new orthophoto map every year. This will create an opportunity for having the most actual TDB, but under the assumption that large amount of data will be effectively analyzed.
The idea of the system is nearly 10 years old; however the system only recently entered the production phase. Private companies, specialized in geodesy, cartography, and photogrametry, are involved in the TBD construction. They perform most of the work on data acquisition as part of these contracts.
As the topographic database is constructed on the base of orthophotomaps, and 10 thousand sheets of orthophotomaps are going to be processed every year, the need for supporting software tools is obvious. Such tools could be used for regions of special interest highlighting, like building, agriculture areas, etc., as well as in the process of database construction and verification. It could be also used for database updating, pointing outs parts of the map that should be updated by comparing the vector map created from the segmented image with the corresponding vector map stored in the TDB.
The applications of neural networks to solve problems in cartography and GIS are already well-established for some time (Meng, 1993; Müller, 1992; Openshaw et al., 1991). In this relatively new, but steady-growing domain, neural networks have been applied to: thematic (semantic) classification of the attributes of objects, classification of spatial objects, aggregation and generalization of objects, and others.
In particular, the applications of neural networks to pattern recognition and land use classification in raster images, particularly satellite images has been considered (Meng, 1993). Most early approaches concentrated on per-pixel classification methods and increasing the spatial accuracy limited by the resolution of available data. Later work concentrated on per-parcel, or per-field, classification by combining the per-pixel techniques with further processing, often statistical classification filters (Berberoglu et al., 2000; German and Gahegan, 1996; Liu et al., 2002; Miller et al., 1995; Tatem et al., 2001; Venkatesh and S. Kumar-Raja, 2003)
This coincides with a broad research field of applying statistical methods in remote sensing: K-means, Gaussian maximum-likelihood, mixture discriminant analysis, fuzzy-c (Abkar et al., 2000; Foody, 2000; Hubert-Moy et al., 2001; Ju et al., 2003; Keuchel et al., 2003; Liu et al., 2002; Pal and Mather, 2003; Stuckens et al., 2000; Venkatesh and S.~Kumar~Raja, 2003) , and Support Vector Machines (SVM) (Bellman and Shortis, 2004).

The idea of identifying textures in raster images appeared early (Haralick, 1979) and has gradually been developed into a mature technology in image processing (Haralick and Shapiro, 1992). It has been recognized as a useful addition to spectral data obtained directly from images to help in the task of segmentation of images (Barr and Barnsley, 1999; Berberoglu et al., 2000; Carr, 1996; Clausi and Zhao, 2002; Haralick and Shapiro, 1992; Ryherd and Woodcock, 1996; Zhang, 1999).

METHODS

Definition of land cover classes used in the topographical maps reflects the character of their use or the role they are playing. Such definition is hardly applicable in the case of aerial orthophotomaps, where whole available information is hidden within colors of raster pixels. The difficulties arise from the fact that areas of the same class may contain objects of different colors, or the objects from different classes may have the same color. Buildings can serve here as an example. Covered with different materials they are seen from the sky as regions of different colors. When covered with asphalt, they might be easily mistaken as roads with the same surface. Hence, for the correct classification, one can consider additional, contextual information. In our case artificial neural networks were used as classifiers. Contextual information appeared indirectly in the training patterns with which the neural networks were fed during the training phase. Thus the use of teacher trained artificial neural networks was a key point in the solution proposed.

Neural networks

The artificial neural networks employed were feed-forward, multi-layer networks trained using hand-crafted reference data. The reference data consisted of aerial photographs accompanied with corresponding images including regions classified by a human operator. To build training patterns two different approaches and/or their combination were used. In the first approach only scaled pixels colors (or intensities) from photographs were taken as inputs. In the second case some local features were computed instead. The local features used in the experiment were texture features computed on the base of gray level co-occurrence matrix (GLCM), which was build after pixels color re-quantization. Apart from that, in both approaches the training patterns were created moving a square mask within a reference image (and/or moving a mask within a feature space) for which expected outputs were collected from an accompanied image. Working with a mask allowed to feed neural network with contextual information indirectly. The size of the input layer of the network was defined by the size of the mask (or size of the feature vector), the size of the output layer was defined by the number of classes provided. The testing patterns were created in a similar manner.

Texture features based on GLCM

Texture might be regarded as what constitutes macroscopic regions. One of the defining qualities of texture is the spatial distribution of gray values. Gray level co-occurrence matrices (GLCM), which estimates image properties related to second-order statistics, have become one of the most well-known and widely used texture features.
The entry of it, which is the number of occurrences of the pair of gray levels which are a distance apart in a given direction, is defines as follows:

$$V_{l,\alpha}(i,j) = \left|\{((r,s),(t,v)) : I(r,s) = i, I(t,v) = j\}\right| \tag{1}$$

where $i, j = 0,\ldots,N-1$; N – number of gray levels; l,α – distance and direction angle; $I(x,y)$ – image pixel at position (x,y); $(t,v) = (r + l\cos\alpha, s + l\sin\alpha)$. Addition of $V_{l,\alpha}$ with its transpose divided by 2 gives symmetrical matrix $\bar{V}_{l,\alpha}$. Symmetrical matrix $\bar{V}_{l,\alpha}$ might be normalized with a total number of pixels in the image before use. These transformations can be written as follows (indices l,α are ommited for convinience) :

$$P_{i,j} = \frac{\bar{V}(i,j)}{\sum_{i,j=0}^{N-1} V(i,j)}, \text{ where } \bar{V}(i,j) = \frac{V(i,j) + V^T(i,j)}{2} . \tag{2}$$

The symmetrical and normalized co-occurrence matrix *P* reveals certain properties about the spatial distribution of the gray levels in the texture image. The features used in experiments are given below:

Texture features based on GLCM					
ASM	energy	entropy	contrast	homogenity	dissimilarity
$\sum_{i,j=0}^{N-1} P_{i,j}^2$	$\sqrt{ASM}$	$\sum_{i,j=0}^{N-1} P_{i,j} \lvert i-j \rvert$	$\sum_{i,j=0}^{N-1} P_{i,j} (i-j)^2$	$\sum_{i,j=0}^{N-1} \frac{P_{i,j}}{1+(i-j)^2}$	$\sum_{i,j=0}^{N-1} P_{i,j} \lvert i-j \rvert$

Processing scheme

The following scheme of processing was applied. At first reference set and testing set were prepared. Each set consisted of aerial photographs of the area of interest and accompanying image with classes assigned. For the local features additional data were constructed. They were computed by preprocessing aerial photographs with a mask.
Next, from the training set the training pattern was created. Artificial neural network was created for a chosen model of architecture. It was trained with a training pattern. After training phase artificial neural network was employed as a classifier. Testing pattern used then was prepared in the same way as the training pattern. The results of classification for the testing set (not used in the training process) and the training set were stored in the resulting images. The resulting images and the accompanying images with classes manually assigned were used to evaluate classification results. For this purpose several different statistical measures have been tried and used (see next subsection).

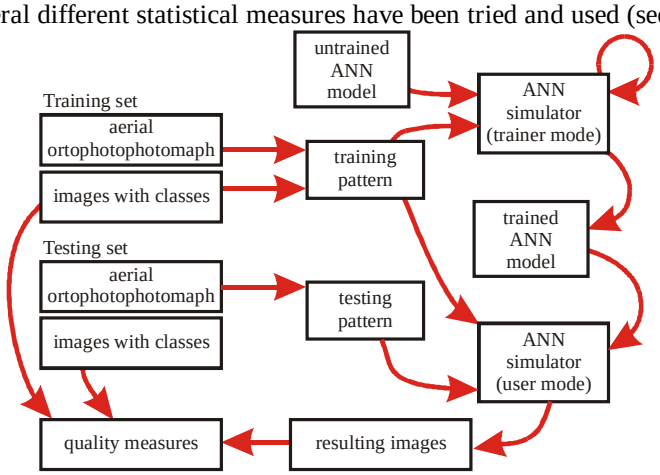

Figure 1. Processing scheme.

Quality measures

To quantify the quality of the results in an automatic manner a confusion matrix $A = \left[a_{ij} \right]$ was created for each case. Element of matrix, a_{ij}, was a number of sample pixels from the *j*th class that have been classified as belonging to the *i*th class. On the base of matrix *A* the following measures have been proposed (Cohen, 1960; Cohen, 1968; Hubert-Moy et al., 2001):

- user's accuracy of class *i*:

$$u_i = \frac{a_{ii}}{a_{ri}} \quad \text{, where } a_{ri} = \sum_i a_{i.} \text{ (sum of } i\text{th row entries);} \tag{3}$$

- producers accuracy of class *i*:

$$p_i = \frac{a_{ii}}{a_{ci}} \quad \text{, where } a_{ci} = \sum_i a_{.i} \text{ (sum of } i\text{th column entries);} \tag{4}$$

- overall accuracy of the method:

$$d = \frac{a_{ii}}{a_t} \quad \text{, where } a_t \text{ is the total number of pixels;} \tag{5}$$

- simple Kappa coefficient:

$$\kappa = \frac{P_o - P_e}{1 - P_e} \quad \text{, where } P_o = \sum_i a_{ii} / a_t \text{ , } P_e = \sum_i a_{ri} a_{ci} / a_t^2 \text{ ;} \tag{6}$$

- weighted Kappa coefficient:

$$\kappa_w = \frac{P_{o(w)} - P_{e(w)}}{1 - P_{e(w)}} \quad \text{, where } P_{o(w)} = \sum_i \sum_j w_{ij} a_{ij} / a_t \ , \ P_{e(w)} = \sum_i \sum_j w_{ij} a_{i.} a_{.j} / a_t^2 \ , \tag{7}$$

and $0 \le w_{ij} < 1$ for all $i \ne j$, and $w_{ij} = 1$ for $i = j$, and $w_{ij} = w_{ji}$;

- averaged error:

$$uDW = \frac{1}{K} \sum_i \varepsilon_i \ \text{, where } \varepsilon_{ij} = \begin{cases} 1 - \dfrac{a_{ij}}{a_{ri}} \ , \ \text{if } a_{ri} > 0 \text{ and } i \ne j \\ 0 \ , \quad \text{otherwise} \end{cases} \ , \ \varepsilon_i = \sum_j \varepsilon_{ij} = \begin{cases} 1 - \dfrac{a_{ii}}{a_{ri}} = 1 - u_i \ , \ \text{if } a_{ri} > 0 \\ 0 \quad , \ \text{otherwise} \end{cases} \ , \tag{8}$$

and K - number of classes.

EXPERIMENTS

The experiments were done with color aerial photographs, taken with 0.5m resolution. Photographs with 1.0m resolution were obtained by the original photographs re-sampling.

Architecture of artificial neural networks used throughout all experiments was dictated by the kind of the experiments performed. Thus the number of units in the networks input layer varied according to the mask and the number of features considered. There were two hidden layers in the networks, with 10 units for each layer. At first the number of units in the output layer matched the number of classes being recognized. Later networks were trained to recognize only one class, thus only one output unit was needed. Because networks classifying several classes simultaneously provided worse results then networks classifying only one class, the networks used in the experiments discussed were networks with one output unit only.

There were two kinds of experiments performed: classifying with a mask moving over color pixels of original photographs, and classifying with in the same source of data supported additionally with texture features computed from GLCM in the region covered by the mask.

For the experiments of the first type the following masks were used: 15x15, 19x19, 31x31, 39x39, 47x47 for the higher resolution, and: 7x7, 9x9, 15x15, 19x19, 23x23 for the lower resolution (dimensions in pixels). There were three classes selected: buildings, roads and forests. This selection reflected objects type in the regional TDB.

For the experiments of the second type the masks used were of size 10x10. GLCM in this case was computed after transforming pixels colors to the gray scale with 32 levels. The co-occurence was search in three directions: 45°, 90°, 135°, 180°, in the distance of 1 pixel. Such texture features as: AMS, energy, entropy, contrast, homogenity, and dissimilarity were computed and averaged. This resulted with 6 values, which were treated as additional inputs to the neural networks.

An example of the training and testing sets used in the first type of experiments are depicted in Figure 2. Squares in the reference images show the areas that corresponds to the results displayed in Figure 4 and Figure 5. An example of the training and testing sets used in the second type of experiments are depicted in Figure 3. Squares there are associated with results of classification collected in Figure 8. Please notice that quality of classification in both cases was evaluated numerically for the whole images (not only for squares shown). Corresponding numbers can be found in the Figure 6, Figure 7, and Figure 9.

	Training set	Testing set
Aerial photographs		

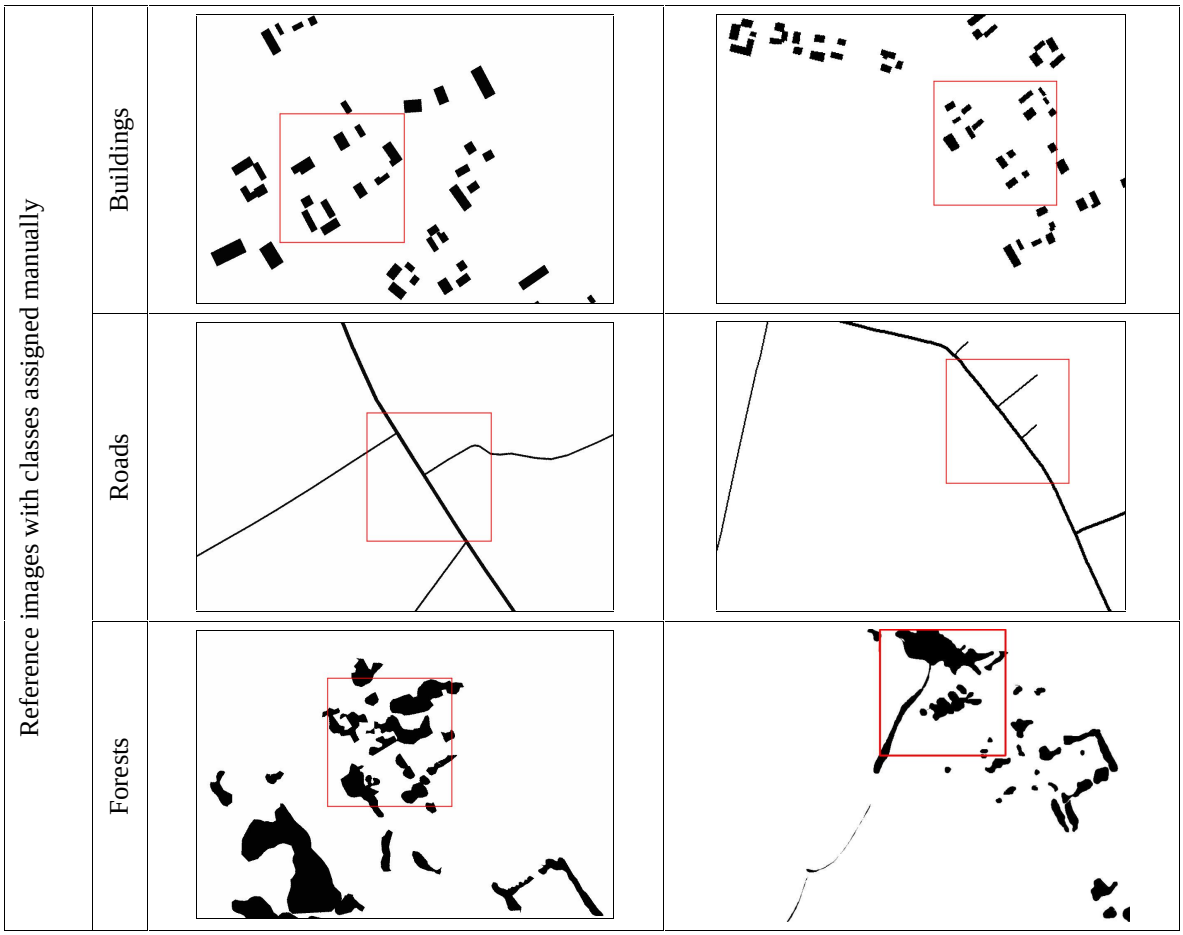

Figure 2. Testing and training sets (aerial photography with accompanying images representing the following classes: buildings, roads, forests)

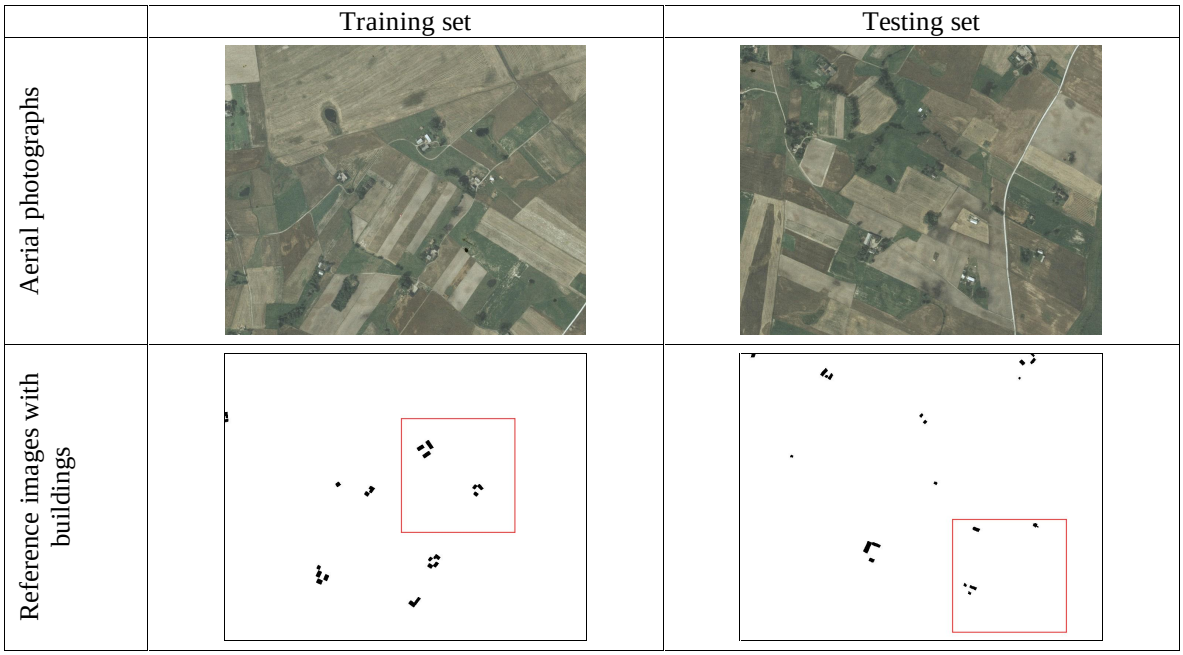

Figure 3. Testing and training sets (aerial photography with accompanying images representing the following classes: buildings, roads, forests)

RESULTS

Classification with the use of masks over color pixels

Results of the training with the use of masks moving over color pixels directly are shown in Figure 4. The results of complementary testing are shown in Figure 5. In both figures only parts of images processed are shown. Each part was a square with 300x300 pixels in size (what in the field was a square with a side width equals 300 m). Numerical evaluations of results are collected in Figure 6 and Figure 7, respectively. Please note, that numbers representing quality measures are computed for the whole images (not for the parts shown).
Results of classification with the use of mask moving over color pixels, which was supported with GLCM based features, are shown in the Figure 8. This figure also contains results of classification without such support. Numerical evaluation of classification results is given in Figure 9.
To distinguish reference images from images representing results of classification former ones are painted in reverse.

Type	Reference image	Results of classification for different masks sizes				
		7x7	9x9	15x15	19x19	23x23
buildings	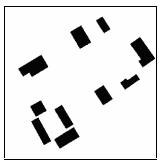					
forests		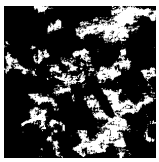		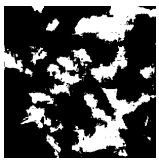	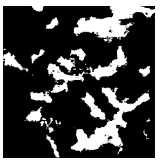	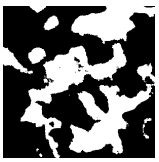
roads	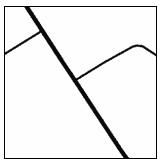					

Figure 4. Classification results for the training set with different mask sizes.

Type	Reference image	Results of classification for different masks sizes				
		7x7	9x9	15x15	19x19	23x23
buildings	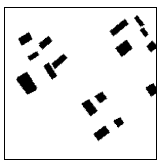	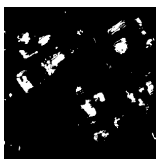	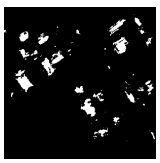			
forests		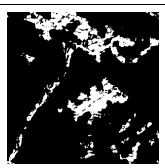	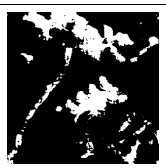	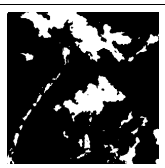	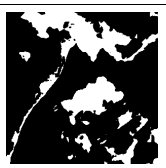	
roads	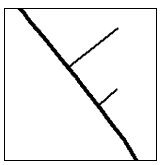	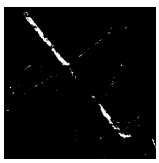	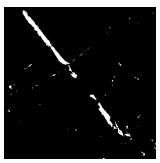			

Figure 5. Classification results for the testing set with different mask sizes.

Type	Mask size	κ_w	u_1	u_2	p_1	p_2	d	uDW
buildings	7x7	0.9778	0.8152	0.9861	0.7481	0.9906	0.9778	0.1987
	9x9	0.9776	0.8406	0.9841	0.7131	0.9925	0.9777	0.1752

	15x15	0.9785	0.8538	0.9846	0.7256	0.9930	0.9786	0.1617
	19x19	0.9786	0.8229	0.9870	0.7709	0.9905	0.9787	0.1901
	23x23	0.9766	0.8313	0.9836	0.7129	0.9917	0.9765	0.1851
roads	7x7	0.9857	0.7983	0.9868	0.2655	0.9988	0.9856	0.2149
	9x9	0.9875	0.8006	0.9893	0.4115	0.9981	0.9876	0.2101
	15x15	0.9851	0.9141	0.9854	0.1944	0.9997	0.9851	0.1006
	19x19	0.9840	0.7103	0.9854	0.2035	0.9985	0.9840	0.3043
	23x23	0.9850	0.8991	0.9853	0.1975	0.9996	0.9849	0.1156
forests	7x7	0.9230	0.6914	0.9484	0.5913	0.9660	0.9233	0.3602
	9x9	0.9289	0.6945	0.9587	0.6792	0.9614	0.9291	0.3468
	15x15	0.9352	0.7269	0.9622	0.7099	0.9652	0.9357	0.3108
	19x19	0.9353	0.7740	0.9516	0.6224	0.9761	0.9350	0.2745
	23x23	0.9224	0.6246	0.9766	0.8314	0.9338	0.9218	0.3988

Figure 6: Numerical evaluation of classification results for the training set. Indices in matrix A: i – class received, j – class provided.

Type	Mask size	κ_w	u_1	u_2	p_1	p_2	d	uDW
buildings	7x7	0.9716	0.9863	0.5534	0.9843	0.5865	0.9715	0.4604
	9x9	0.9726	0.9900	0.4831	0.9819	0.6298	0.9727	0.5270
	15x15	0.9736	0.9883	0.5587	0.9843	0.6303	0.9735	0.4529
	19x19	0.9726	0.9902	0.4838	0.9817	0.6397	0.9727	0.5260
	23x23	0.9638	0.9734	0.6998	0.9890	0.4863	0.9638	0.3269
roads	7x7	0.9837	0.9984	0.1166	0.9852	0.5459	0.9836	0.8850
	9x9	0.9837	0.9973	0.1820	0.9863	0.5363	0.9837	0.8207
	15x15	0.9850	0.9996	0.1128	0.9852	0.8431	0.9849	0.8876
	19x19	0.9841	0.9999	0.0378	0.9840	0.9375	0.9840	0.9622
	23x23	0.9844	0.9989	0.1310	0.9856	0.6599	0.9845	0.8701
forests	7x7	0.9464	0.9711	0.5446	0.9723	0.5336	0.9467	0.4843
	9x9	0.9458	0.9633	0.6616	0.9791	0.5230	0.9460	0.3751
	15x15	0.9430	0.9604	0.6607	0.9789	0.5051	0.9432	0.3789
	19x19	0.9395	0.9527	0.7193	0.9823	0.4822	0.9392	0.3281
	23x23	0.9441	0.9622	0.6566	0.9786	0.5164	0.9446	0.3812

Figure 7. Numerical evaluation of classification results for the testing set. Indices in matrix A: i – class received, j – class provided.

Type	Reference image	Results of classification for different features	
		GLCM+RGB	RGB
buildings (training set)	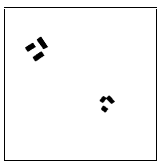		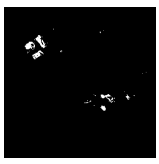
buildings (testing set)	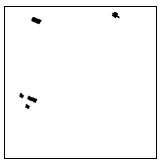	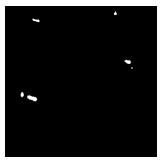	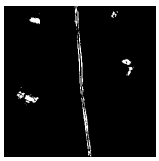

Figure 8. Classification results for the training and testing sets with different sources of features (GLCM+RGB, RGB).

Type	Features	κ_w	u_1	u_2	p_1	p_2	d	uDW
buildings (training set)	GLCM+RGB	0.9966	0.5532	0.9986	0.6353	0.9980	0.9966	0.4482
	RGB	0.9974	0.5339	0.9995	0.8202	0.9979	0.9974	0.4666
buildings (testing set)	GLCM+RGB	0.9972	0.2345	0.9997	0.7218	0.9975	0.9973	0.7657
	RGB	0.9932	0.4707	0.9949	0.2318	0.9983	0.9932	0.5344

Figure 9. Numerical evaluation of classification results for for the training and testing sets with different sources of features (GLCM+RGB, RGB). Indices in matrix A: i – class provided, j – class received.

CONCLUSIONS

The experiments described in this paper have been conducted with color aerial photographs of 1m and 0.5m resolutions, and different neural networks architectures. The results from these experiments were successful (good or excellent) for some types of spatial features, such as water and some types of forests, satisfactory for some other features (fields), and barely acceptable for still other features, such as urban areas or roads. However, a strong correlation was observed between the neural network (mask) size and the size of the objects of interest.

The experiments performed demonstrated, that optimal masks sizes are correlated with the characteristic of the area classified. It appeared, for example, that for roads detection the mask width (and height) should be such as the road width.

It was observed, that reduction of the photographs scale does not seriously deteriorate the results of classification, but significantly reduce the computational complexity of the task (smaller masks might be used).

It appeared that masks greater then 19x19 for photographs 1000x600 with resolution 0.5m were not reasonable with respect to the computation time (for PC with Intel Pentium 4 1.7 GHz processor).

Combining texture features with mask processing of color pixels decrease the number of pixels from outside of some class incorrectly assigned to that class, which means that false classification rate is reduced. But it also decreases the number of pixels, which should be classified as class members, which means that positive classification rate is also reduced. This result is generally undesired, apart from one fact. Pixels assignment to classes under classification supported by the texture features are more reliable then pixels assigned to the class without this support. This can be observed in Figure 8 (buildings - testing set), where parts of the roads were misclassified as buildings without use of texture features, whereas use of texture features allowed eliminating such artifacts.

REFERENCES

Abkar, A.-A., Sharifi, M.A. and Mulder, N.J., 2000. Likelihood-based image segmentation and classification: a framework for the integration of expert knowledge in image classification procedures. International Journal of Applied Earth Observation and Geoinformation, 2(2): 104-119.

Barr, S. and Barnsley, M.J., 1999. A syntactic pattern recognition paradigm for the derrivation of second-order thematic information from remotely sensed images. In: P.M. Atkinson and N.J. Tate (Editors), Advances in Remote Sensingand GIS Analysis. Chichester: WIley, pp. 167-184.

Bellman, C.J. and Shortis, M.R., 2004. A classification approach to finding buildings in large scale aerial photographs, XXth ISPRS Congress, Istanbul, Turkey.

Berberoglu, S., Lloyd, C.D., Atkinson, P.M. and Curran, P.J., 2000. The integration of spectral and textural information using neural networks for land cover mapping in the Mediterranean. Computers and Geosciences, 26(4): 385-396.

Carr, J.R., 1996. Spectral and textural classification of single and multiple band digital images. Computers and Geosciences, 22(8): 849-865.

Clausi, D.A. and Zhao, Y., 2002. Rapid extraction of image texture by co-occurrence using a hybrid data structure. Computers and Geosciences, 28(6): 763-774.

Cohen, J., 1960. A Coefficient of Agreement for Nominal Scales. Educational and Psychological Measurement, 20: 37-46.

Cohen, J., 1968. Weighte kappa: nominal scale agreement wit provision for scale disagreement or partial credit. Psychol. Bull., 70: 213-220.

Foody, G.M., 2000. Estimation of sub-pixel land cover composition in the presence of untrained classes. Computers and Geosciences, 26(4): 469-478.

German, G.W.H. and Gahegan, M.N., 1996. Neural network architectures for the classification of temporal image sequences. Computers and Geosciences, 22(9): 969-979.

Haralick, R.M., 1979. Statistical and structural approaches to texture. Proceedings of IEEE, 67(5): 786-803.

Haralick, R.M. and Shapiro, L.G., 1992. Computer and Robot Vision, vol. 1., 1. Addison-Wesley Publishing, Reading, MA.

Hubert-Moy, L., Cotonnec, A., Du, L.L., Chardin, A. and Perez, P., 2001. A Comparison of Parametric Classification Procedures of Remotely Sensed Data Applied on Different Landscape Units. Remote Sensing of Environment, 75(2): 174-187.

Ju, J., Kolaczyk, E.D. and Gopal, S., 2003. Gaussian mixture discriminant analysis and sub-pixel land cover characterization in remote sensing. Remote Sensing of Environment, 84(4): 550-560.

Keuchel, J., Naumann, S., Heiler, M. and Siegmund, A., 2003. Automatic land cover analysis for Tenerife by supervised classification using remotely sensed data. Remote Sensing of Environment, 86(4): 530-541.

Liu, X.-H., Skidmore, A.K. and H. Van Oosten, 2002. Integration of classification methods for improvement of land-cover map accuracy. ISPRS Journal of Photogrammetry and Remote Sensing, 56(4): 257-268.

Meng, L., 1993. Application of neural network in cartographic pattern recognition, Proccedings 16th International Cartographic Conference, Cologne, pp. 192-202.

Miller, D.M., Kaminsky, E.J. and Rana, S., 1995. Neural network classification of remote-sensing data. Computers and Geosciences, 21(3): 377-386.

Müller, J.-C., 1992. Parallel distributed processing: An application to geographic
feature selection, Proceedings Fifth International Symposium on Spatial Data Handling, Charleston, SC, pp. 230-240.

Openshaw, S., Wymer, C. and Cross, A., 1991. Using neural nets to solve some hard analysis problems in GIS, Proceedings EGIS '91, Brussels, pp. 797-807.

Pal, M. and Mather, P.M., 2003. An assessment of the effectiveness of decision tree methods for land cover classification. Remote Sensing of Environment, 86(4): 554-565.

Ryherd, S. and Woodcock, C., 1996. Combining spectral and texture data in the segmentation of remotely sensed images. Photogramm. Eng. Remote Sens., 62: 181-194.

Stuckens, J., Coppin, P.R. and Bauer, M.E., 2000. Integrating Contextual Information with per-Pixel Classification for Improved Land Cover Classification. Remote Sensing of Environment, 71(3): 282-296.

Tatem, A.J., Lewis, H.G., Atkinson, P.M. and Nixon, M.S., 2001. Super-Resolution Target Identification from Remotely Sensed Images using a Hopfield Neural Network. IEEE Transactions on Geoscience and Remote Sensing(39): 781-796.

Venkatesh, Y.V. and S. Kumar Raja, 2003. On the classification of multispectral satellite images using the multilayer perceptron. Pattern Recognition, 36(9): 2161-2175.

Zhang, Y., 1999. Optimisation of building detection in satellite images by combining multispectral classification and texture filtering. ISPRS Journal of Photogrammetry and Remote Sensing, 54(1): 50-60.